Journal of Advanced Ceramics
2013, 2(3): 218–226
DOI: 10.1007/s40145-013-0063-z

ISSN 2226-4108
CN 10-1154/TQ

Research Article

Structural and photocatalytic characteristics of TiO_2 coatings produced by various thermal spray techniques

Pavel CTIBOR[a,*], Vaclav STENGL[b], Zdenek PALA[a]

[a]*Institute of Plasma Physics, ASCR, v.v.i., Za Slovankou 3, Prague, Czech Republic*
[b]*Institute of Inorganic Chemistry, ASCR, v.v.i., Husinec-Rez, Czech Republic*

Received: January 09, 2013; Revised: April 10, 2013; Accepted: April 15, 2013

Abstract: Titanium dioxide (TiO_2) was elaborated by four different thermal spray techniques—(i) plasma spraying using a water-stabilized torch, (ii) plasma spraying using a gas-stabilized torch, (iii) high velocity oxy–fuel gun, and (iv) oxy–acetylene flame. The porosity of the coatings was studied by optical microscopy, nano-structural features by scanning electron microscopy (SEM), phase composition by X-ray diffraction (XRD); the microhardness, surface roughness and wear resistance were evaluated. The diffuse reflectance was measured by ultra-violet/visible/near-infrared (UV/Vis/NIR) scanning spectrophotometer. The kinetics of photocatalytic degradation of gaseous acetone was measured under a UV lamp with 365 nm wavelength. After all the applied spray processes, the transformation of anatase phase from the initial powders to rutile phase in the coatings occurred. In spite of this transformation, all the coatings exhibited certain photocatalytic activity, which correlated well with their band gap energy calculated from reflectivity. All the coatings offer relatively good mechanical properties and can serve as robust photocatalysts.

Keywords: plasma spraying; high velocity oxy–fuel (HVOF) spraying; flame spraying; titanium dioxide (TiO_2); photocatalysis; band gap

1 Introduction

Titanium dioxide (TiO_2) photocatalyst has emerged as a promising clean advanced oxidation technology, which could address the ever-increasing global concerns for environmental pollution. TiO_2 is an important material for ultra-violet (UV) assisted photocatalysis in the state of fine powders [1–3], thin coatings [3,4] as well as thermally sprayed coatings [5–9], and useful for water and air purification in advanced electrochemical applications. The demand for robust photocatalytic layers is initiated with multiple technical problems in handling with ultrafine powders and thin coatings. Here is a challenge for thermal spray techniques.

The thermal spray techniques used for the current work differ markedly in temperature, gases participating in the employed chemical processes, particle velocity and feed rate, etc. All these factors have influence on the resulting coatings [10–13].

The **high velocity oxy–fuel** (HVOF) process utilizes a combination of oxygen with various fuel gases, including hydrogen, propane, propylene, and kerosene. In the combustion chamber, burning products are expanded and expelled outward through an orifice with very high velocities. Powders to be sprayed via HVOF

* Corresponding author.
E-mail: ctibor@ipp.cas.cz

are injected axially into the expanding hot gases where they are propelled forward, heated and accelerated onto a surface to form a coating. Gas velocities are supersonic, whereas the temperature is about 2300 ℃. The coupling of highly plasticized particles can achieve coatings approaching the theoretical density. Disadvantages include relatively low deposition rates. Recent efforts have been focused on applying thick coatings and improvements in the process control.

Powder **flame spraying** is probably the simplest of all the spray processes—powders are fed through the center bore of a nozzle where they melt and are carried by the escaping oxy–fuel gases to the work piece. Unfortunately, this approach yields coatings with high porosity content. The density of the supporting gas influences the feed rate, and there is an optimum amount that can be carried in a gaseous stream for any particular powders. It depends on the velocity and volume of the gases used.

Plasma is an ionized gaseous jet composed of free electrons, positive ions, neutral atoms and molecules. In a commercial technology, plasma is considered a hot stream reaching temperatures greater than 10 000 ℃. The generator is essentially an electric arc working in a constricted space. Two electrodes, front (anode) and rear (cathode), are contained in a chamber, as is the arc through which the operating gas passes. Plasma generators work on the principle that—if sufficient voltage is applied to the two electrodes, separated by a small gap—the gas in the gap is ionized, becoming electrically conductive. Plasma subsequently exits the chamber as a plasma jet. This concept represents a **gas-stabilized plasma** (GSP) torch.

Water-stabilized plasma (WSP) torch has the advantage of combining stabilizing system and cooling system in one. Water is fed into a chamber instead of gases, where it creates a swirl around the walls. Electric arc is burning in the center of the channel formed by the swirl, between the graphite cathode inside the chamber and a rotating copper anode outside. The anode is internally water-cooled. Feedstock powders are introduced into the plasma jet outside the gun using two injectors, which can be positioned in various distances (feeding distance, FD) from the exit nozzle. The oxidizing power of oxygen released from the water is balanced by the reducing power of hydrogen, thus the overall chemical influence of the stabilizing water in the flame is rather neutral. In general, the structures of coatings made by GSP and WSP are relatively similar.

The main goal of the present paper is to investigate spraying TiO_2 by all techniques described above. TiO_2 represents a ceramic material with moderate refractory character, medium hardness and toughness. It is—according to our previous experience (mainly based on WSP spraying)—suitable for thick coatings. From the coating's mechanical integrity point of view, TiO_2 is relatively insensitive to spraying parameters; however, it is sensitive to reduction, undergoes phase transformation at cooling, and its numerous physical properties can be tailored only after studying the phenomena associated with the individual spraying methods.

2 Experiment

2.1 Powders and spraying

TiO_2 powder feedstock for thermal spray (Altair Nanomaterials, Reno, NV, USA) was prepared from nanometric (~ 20 nm) powders by agglomeration. The fraction of 75–106 μm in size was utilized for WSP spraying experiments. Samples were produced using the spraying system WSP 500 (Institute of Plasma Physics, Prague, Czech Republic). Carbon steel as well as stainless steel coupons was used as substrates. Some of the coatings were then stripped off for further characterizations. The spraying parameters of WSP are in Table 1. Argon was used as a powder feeding gas—a pressure of 2.5 bar and a flow rate of 3.25 slpm were employed. Argon was also used for cooling the substrate and the just deposited coating. The cooling tube was installed on a robot, and after each pass, it copied the movement pattern of the spray gun over the substrate. The temperature was monitored by a two-color pyrometer not to exceed 250 ℃.

An overview of the used spraying parameters for all other techniques is also presented in Table 1. Where not indicated, compressed air was used as the powder feeding gas. TopGun Medipar 02–555 (Medicoat, Maegenwil, Switzerland) was used for HVOF, plasma torch Plasmatechnik F4 (Sulzer Metco, Winterthur, Switzerland) was used for GSP spraying, and conventional flame spray equipment was employed. All processes other than WSP were performed at SAM Ltd. (Miletin, Czech Republic).

Table 1 Parameters used for spraying

Process	Feeding distance, FD (mm)	Spray distance, SD (mm)	Torch power (kW)	Gases used	Substrate temperature (℃)	Powder feed rate (kg/h)	Feedstock powder size (μm)	Feedstock anatase content (%)**
WSP	120	400	150	H_2O vapor, Ar feeding	250	15	75–106	95
GSP	—	130	9	Ar + H_2 (80/35*), Ar feeding	130	3	20–50	77
HVOF	—	220	—	oxygen, ethylene C_2H_4; N_2 feeding	170	1.2	75–106	95
Flame	—	220	—	oxygen, acetylene C_2H_2	—	—	20–50	77

* flow rates in standard liters per minute; ** the balance is rutile.

Different size distributions of the powders for the different spraying techniques are necessity. The fact that TiO_2 powders with different sizes also have different anatase contents (verified by X-ray diffraction (XRD)) is a producer-governed feature, difficult to avoid if we work with a commercial material.

The parameters for spraying with various techniques were selected having in mind the main target to obtain coatings relatively comparable with the WSP coating from the viewpoint of the oxygen non-stoichiometry. At both GSP and WSP spraying, titania is usually reduced and the coating has a lower content of oxygen compared to the starting powders [14]. In the case of our GSP spraying, a very low power level was selected as a means contributing to the oxygen loss. Low power level represented a low powder temperature. Low feed rate was used at the same time. A small quantity of powder particles in a plasma plume with low temperature was supposed to maximize the influence of plasma-constituent gases and minimize the influence of the ambient air surrounding the plasma plume. The temperature of substrate was kept relatively low (150 ℃) to support cooling. As a result, oxygen-deficient coating was expected.

HVOF parameters were selected also with the aim to support reduction of the powders. Relatively low feed rate was used together with nitrogen as a powder feeding gas, both with the aim to limit the contact of the powders with the ambient air.

For the same reason, a reductive flame with high acetylene-to-oxygen ratio was applied in the case of flame spraying.

2.2 Characterization techniques

The porosity was studied by optical microscopy on polished cross sections. The micrographs were taken with a CCD (charge-coupled device) camera and processed using an image analysis (IA) software (Lucia G, Laboratory Imaging, Czech Republic). Ten images of microstructures taken from various areas of the cross section for each sample were analyzed. The magnification was 250 in all cases. For a better description of the porosity, certain additional criteria were introduced [16].

The microstructures of selected coatings were also studied by a scanning electron microscope (SEM) EVO® MA 15 (Carl Zeiss SMT Inc., Germany) with point resolution of 2 nm at 30 kV. TiO_2 coatings made by GSP were analyzed also by high-resolution transmission electron microscope (HR-TEM) Jeol JEM 3010.

XRD was performed on a 2-theta Bragg–Brentano diffractometer SIEMENS D500, using cobalt Kα radiation to obtain information about the phases present in the feedstock powders and coatings. A "beamknife" attachment improving the peak-to-background ratio was employed.

The microhardness was measured by a Hanemann microhardness head (Carl Zeiss, Germany) mounted on an optical microscope with a fixed load of 1 N and a Vickers indenter. Twenty indentations in various areas of the cross section for each sample were made.

The slurry abrasion response (SAR) of coatings was measured based on an ASTM standard [17] using an in-house designed apparatus. SAR test was based on measuring the mass loss rate of a standard-shaped block (7.5 mm × 12 mm × 25 mm) lapped in slurry. The test was run for 8 h in 2 h increment with mass loss being measured at the end of each increment. The applied force was 22 N per specimen. After each run, the samples were ultrasonically cleaned and weighted. The slurry consisted of 150 g water and 150 g alumina

powders having size of 40–50 μm. The accuracy of measurement was approximately ±5%. The parameter "inverse wear rate" was higher for a coating with better wear resistance.

The diffuse reflectance was measured by an ultraviolet/visible/near-infrared (UV/Vis/NIR) scanning spectrophotometer (Shimadzu, Japan) with a multipurpose large sample compartment. Prior to the actual measurement, the calibration was conducted using the $BaSO_4$ reference mirror in order to minimize the possible error from the experimental environment. The measurement accuracy guaranteed by the equipment manufacturer was as follows: the accuracy of wavelength was less than ±0.3 nm, and the uncertainty of the measurement was less than 0.2%. The wavelength of incident light used for the reflectance measurement was in the range from 250 nm to 2000 nm, and the diameter of the measured area was about 20 mm. The corresponding band gap width was estimated based on the values converted to absorbance and recalculated to band gap energy E_{bg} [18].

The kinetics of photocatalytic degradation of gaseous acetone was measured using a self-constructed stainless steel photoreactor with a fluorescent lamp Narva LT8WT8/073BLB and a black lamp with a wavelength of 365 nm and input power of 8 W (light intensity 6.3 mW/cm^2). The gas concentration was measured with a quadrupole mass spectrometer JEOL JMS-Q100GC and gas chromatograph Agilent 6890N. A high-resolution gas chromatography column (19091P-QO4, J&W Scientific) was used. The sample from the reactor was taken via a sampling valve at a time interval of 2 h. The reactor with a total volume of 3.5 L was filled with oxygen at a flow rate of 1 L/min.

3 Results and discussion

The microstructures of coatings are shown in Figs. 1(a)–1(d). The coatings have different thicknesses—only about 150 μm for HVOF and flame spraying, whereas plasma-sprayed coatings are markedly thicker.

The HVOF coating contains unmelted particles with nano-structure exhibiting several tens of nanometer-large individual particles separated by fine pores (Fig. 2(a)). The structure of this coating is bimodal, similar to another publication [15]—besides the mentioned nanostructural particles, the rest of the coating exhibits a microstructure with splats built from completely resolidified TiO_2. This feature is not observed in any

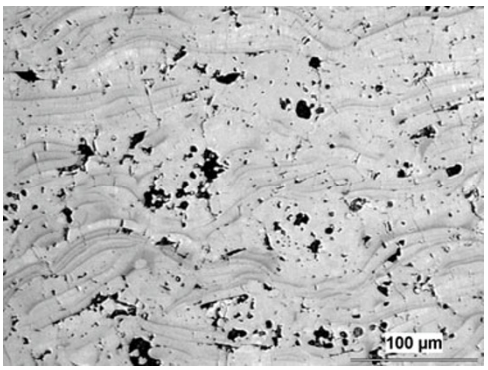

(a)

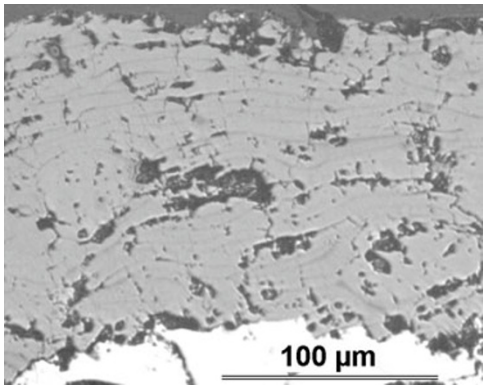

(b)

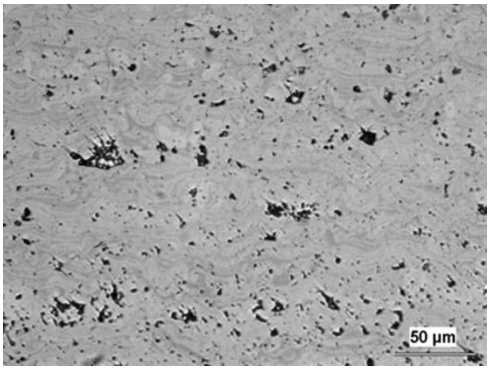

(c)

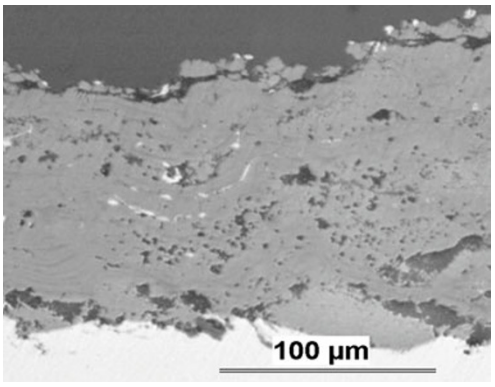

(d)

Fig. 1 Optical microscopy of the cross-sections of (a) WSP coating, (b) flame-sprayed coating, (c) GSP coating, and (d) HVOF coating.

other coatings in our set of experiments. The reason is that the high velocity of the particles impacting under relatively cold conditions onto the substrate, results in the disintegration of the agglomerated powders.

Certain splat-to-splat variability of the level of grey is visible in the GSP coating (Fig. 2(b)), most probably associated with the subtle variation in stoichiometry. The WSP and flame-sprayed coatings exhibit some globular particles disturbing the general arrangement of lamellas aligned perpendicularly to the spraying direction. Such particles are not flattened well at impact because of the low impact velocity, but they retain the original size and shape of the feedstock.

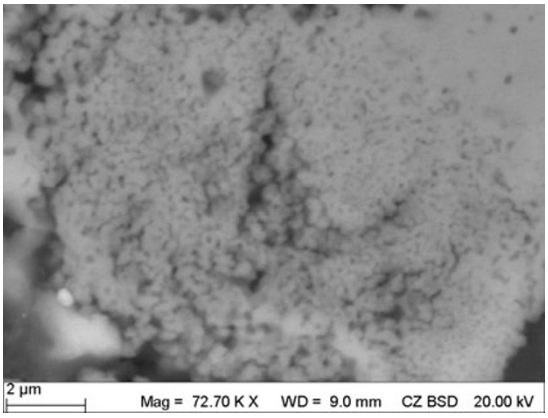

(a)

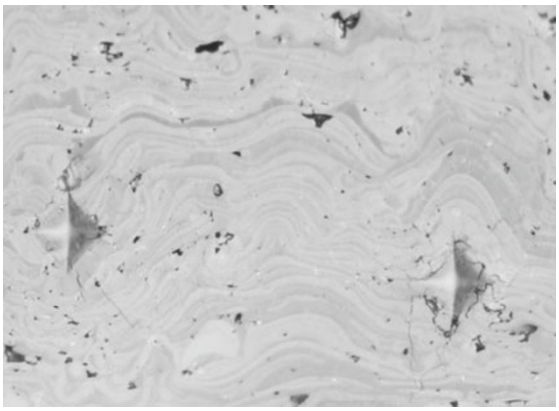

(b)

Fig. 2 (a) Detail of the cross section of HVOF coating; (b) detail of two indents on the cross section of the GSP coating.

The surface roughness is the biggest for WSP coating and similar for all other coatings (smaller than WSP) (Table 2). Finer starting powders lead typically to finer roughness, and comparing the particle impact velocity of WSP and HVOF, the second one is markedly higher leading to finer roughness. The porosity is similar for WSP and flame-sprayed coatings, whereas it is lower for HVOF and even lower for GSP. The mean pore size for HVOF is the lowest due to a large impact velocity resulting in good splat contact, whereas for all other coatings it is similar. The pores are globular particularly for GSP and HVOF, whereas for WSP and flame spray, they are flatter (lower minimal circularity). This is probably due to a low feed rate used at HVOF and GSP spraying enabling more homogeneous melting of the powders, particularly in the case of GSP.

In the case of HVOF, low microhardness is in connection with the bimodal zones depicted in Fig. 2(a). The wear resistance of the HVOF coating is also the worst, being less than one half of the best value obtained with the GSP coating. The inverse wear rate values have the same trend as microhadrdness. In fact, HVOF spraying of ceramics needs relatively sophisticated optimization [15] to get perfect melting of the powders and building of the coating with this low-temperature process leading to good mechanical properties. Plasma spraying offers better melting of the ceramic powder particles (indicated by low roughness), resulting in good inter-splat contact in the coatings. That is why they exhibit higher microhardness than flame and HVOF coatings. Also, the lower standard deviation of the microhardness values obtained for both plasma-sprayed coatings (compared to flame and HVOF) is due to better homogeneity of well bonded

Table 2 Characteristics of the coatings

Parameter	WSP	GSP	HVOF	Flame
Phase according to XRD	Rutile	Rutile	Rutile	Rutile
E_{bg} at indirect transition (eV)	3.12 (2.22)	3.08	2.82 (2.34)	3.25
Surface roughness R_a (μm)	13.4 ± 0.5	4.3 ± 0.14	5.7 ± 0.2	5.9 ± 1.4
Surface roughness $R_{y,max}$ (μm)	97.7 ± 6.4	35.2 ± 3.8	50.6 ± 4.7	48.8 ± 2.4
Porosity (%)	8.5	3.4	4.4	8.3
Mean pore size (μm)	13.6	12.9	7.8	13.9
Pore circularity minimum	0.095	0.144	0.158	0.051
Microhardness at 1 N (GPa)	9.46 ± 1.31	10.40 ± 1.60	4.95 ± 2.11	8.42 ± 2.35
Inverse wear rate (m/mm^3)	29.3	50.1	18.4	21.7

splats.

From the viewpoint of wear resistance, the GSP coating is markedly superior over all other coatings. This is mainly because of its low porosity. The HVOF coating is the worst; its porosity is also relatively low, but its bimodal structure exhibits defects like clusters of pores, particularly near the substrate (Fig. 1(d)).

According to the XRD in all coatings, the only identified phase is rutile (Fig. 3). The difference in the intensities of peaks corresponding to rutile planes (indicated in the top image) is due to the different surface qualities of samples. The absence of peaks of known sub-stoichiometric titanium oxides is due to the fact that an oxygen-deficient structure can be, besides sub-stoichiometric titanium oxides, also formed predominantly by vacancies [19,20] and crystallographic stacking faults [14]. In the HR-TEM micrograph (Fig. 4(a)), a region with point defects is marked by a circle. In Fig. 4(b), a crystallographic stacking fault is aligned in the direction of the long arrow and creates a misalignment between the crystal planes marked by short arrows.

As a result of the photocatalytic test, the relative concentration of the substances $C/C(0)$, where $C(0)$ is the initial concentration, is displayed versus time (Fig. 5). The HVOF and GSP coatings have very similar photocatalytic characteristics.

Under the UV light among all coatings, a 10% degradation of acetone within 16 h is reached by the GSP and HVOF coatings. At the same time, WSP and flame coatings reach 6% and 3% of acetone decomposition, respectively (Fig. 5(a)). The CO_2 uptake is relatively similar for all coatings with exception of the flame coating (Fig. 5(b)). Also, the CO uptake is relatively similar for HVOF, WSP and GSP coatings, while for the flame coating it is again significantly higher (Fig. 5(c)).

Band gap energies are the lowest for HVOF and GSP, 2.82 eV and 3.08 eV respectively (Fig. 6). The WSP coating is proven as a medium quality photocatalyst among the studied coatings. Also, its band gap is slightly higher, 3.12 eV. Finally, the flame-sprayed coating is the least photoactive one and its band gap energy is the highest, 3.25 eV. For the HVOF and WSP coatings, secondary absorption edges also exist at 2.34 eV and 2.22 eV, respectively. The

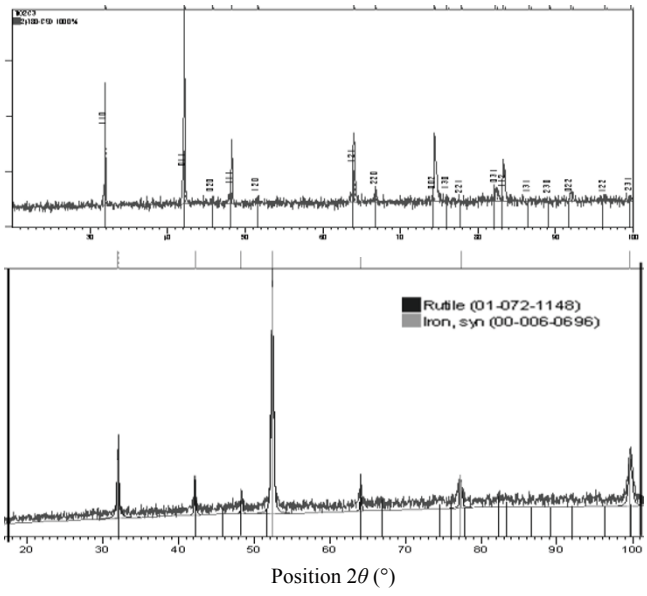

Fig. 3 XRD patterns of flame-sprayed coating (top) and HVOF coating (bottom).

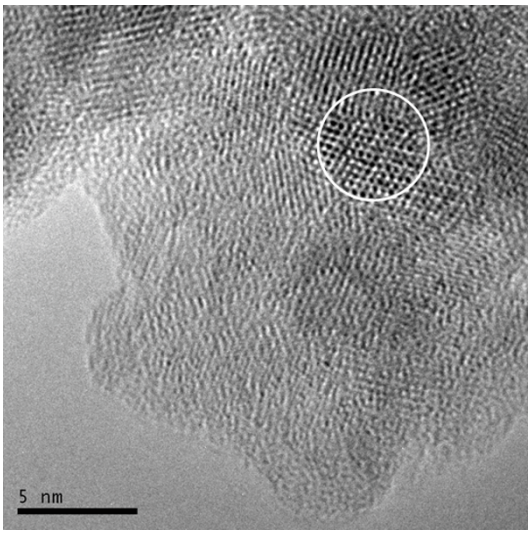

(a)

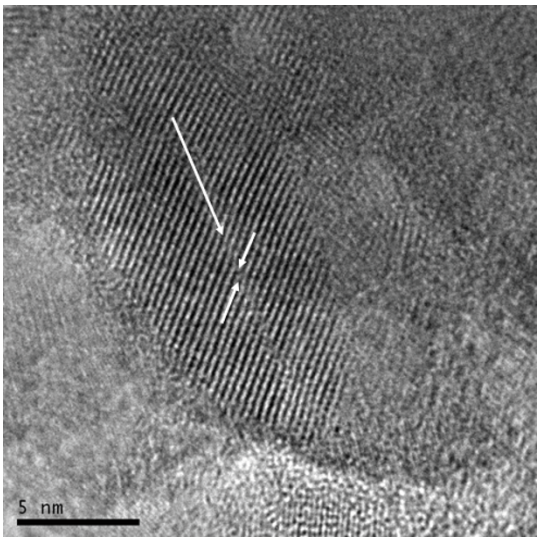

(b)

Fig. 4 HR-TEM micrographs of (a) point defects and (b) stacking fault in GSP TiO_2 coating.

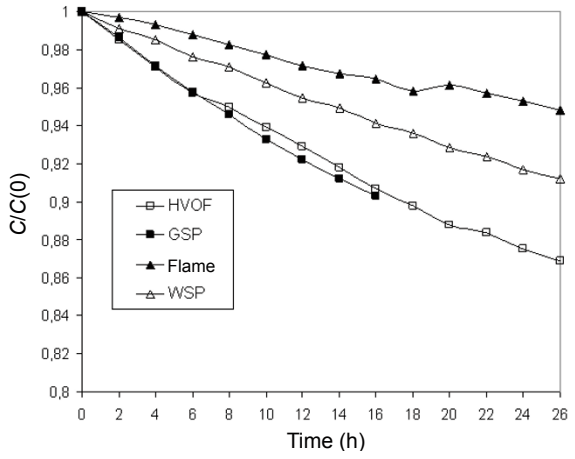

(a)

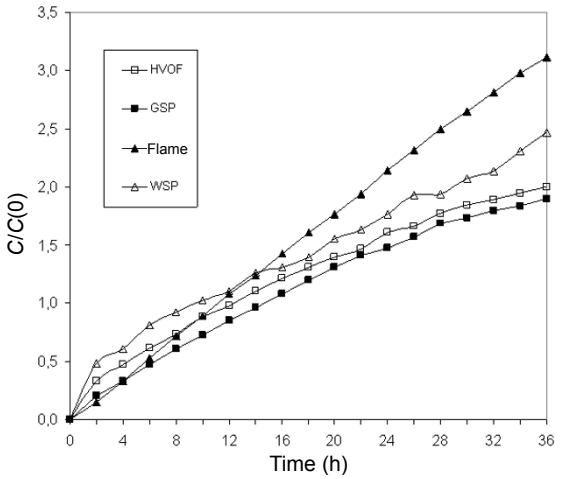

(b)

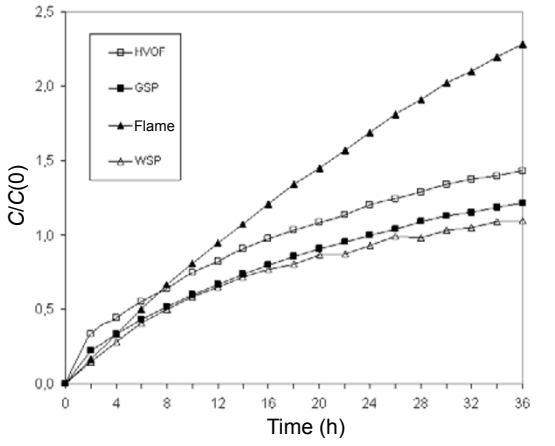

(c)

Fig. 5 Kinetics of (a) acetone concentration decrease, (b) carbon dioxide concentration increase, and (c) carbon monoxide concentration increase.

main absorption edge at $E_{bg}(1)$ corresponds to non-stoichiometric TiO_2 features in rutile, and the secondary absorption edge at $E_{bg}(2)$ corresponds to an absorption tail of delocalized electronic states with a low excitation energy [19,21,22]. The existence of a secondary absorption edge does not seem to correlate tightly with the acetone photo-decomposition.

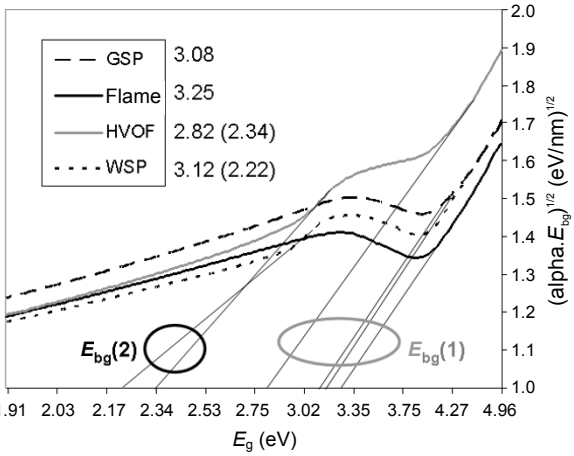

Fig. 6 Band gap estimation for all coatings. The energies of primary (and secondary) absorption edge (eV) are in the legend.

GSP spraying process due to H_2 and HVOF spraying process due to ethylene both provide more free hydrogen atoms for reactions leading to the reduction of TiO_2. In the case of WSP and flame spraying, the working gas does not provide efficient conditions for reduction. Anatase is more sensitive to reaction with hydrogen from ethylene C_2H_4 than from acetylene C_2H_2 [23,24]. Anatase is present in higher content in the feedstock for HVOF spraying than in the feedstock used for flame spraying. That is why the flame-sprayed coating should have less oxygen-deficiency than the HVOF coating and therefore less photoactivity. Concerning the GSP coating, the high rutile content in the feedstock exhibits the possibility to be highly reduced directly by H_2 plasma gas. Flame coating has the highest band gap, and according to previous considerations, it should be less oxygen-deficient.

4 Conclusions

TiO_2 was sprayed by four different thermal spraying techniques—plasma spraying using a water-stabilized torch, plasma spraying using a gas-stabilized torch, high velocity oxy–fuel gun, and oxy–acetylene flame. Plasma spraying was realized with high coating thickness. The last two techniques—usually considered as non-optimal for spraying ceramics because they exhibited significantly lower temperature accessible with the heating medium—were employed successfully,

too. The target of our work was to obtain all coatings with the main feature typical for plasma spraying of TiO_2, i.e., oxygen-deficient structure. The other feature inherent to all applied spray processes was the transformation of anatase phase in the initial powders to rutile phase in the coatings. In spite of this transformation, all coatings exhibited certain photocatalytic activity, which correlated well with their band gap energy. This feature was present thanks to the oxygen-deficient structure exhibiting vacancies and crystallographic stacking faults. At the same time, all the coatings offer relatively good mechanical properties and can serve as robust photocatalysts.

All techniques used also offered processing parameter ranges suitable for further optimization of titania spraying especially from the viewpoint of the mechanical integrity of the coatings. At GSP, the very low feed rate used brought good photocatalytic performance and good mechanical properties, whereas the HVOF coating, having GSP-similar photoactivity, was mechanically inferior. This fact resulted from the markedly different jet temperatures for these two techniques.

Acknowledgements

This work was supported by the Czech Science Foundation under Project P108/12/1872.

References

[1] Li D, Haneda H, Hishita S, *et al*. Fluorine-doped TiO_2 powders prepared by spray pyrolysis and their improved photocatalytic activity for decomposition of gas-phase acetaldehyde. *J Fluorine Chem* 2005, **126**: 69–77.

[2] Matsuda S, Hatano H, Tsutsumi A. Ultrafine particle fluidization and its application to photocatalytic NO_x treatment. *Chem Eng J* 2001, **82**: 183–188.

[3] Herrmann J-M. Heterogeneous photocatalysis: Fundamentals and applications to the removal of various types of aqueous pollutants. *Catal Today* 1999, **53**: 115–129.

[4] Dumitriu D, Bally AR, Ballif C, *et al*. Photocatalytic degradation of phenol by TiO_2 thin films prepared by sputtering. *Appl Catal B*: *Environ* 2000, **25**: 83–92.

[5] Colmenares-Angulo J, Zhao S, Young C, *et al*. The effects of thermal spray technique and post-deposition treatment on the photocatalytic activity of TiO_2 coatings. *Surf Coat Technol* 2009, **204**: 423–427.

[6] Ctibor P, Pala Z, Sedláček J, *et al*. Titanium dioxide coatings sprayed by a water-stabilized plasma gun (WSP) with argon and nitrogen as the powder feeding gas: Differences in structural, mechanical and photocatalytic behavior. *J Therm Spray Techn* 2012, **21**: 425–434.

[7] Ctibor P, Štengl V, Píš I, *et al*. Plasma sprayed TiO_2: The influence of power of an electric supply on relations among stoichiometry, surface state and photocatalytic decomposition of acetone. *Ceram Int* 2012, **38**: 3453–3458.

[8] Ctibor P, Stengl V, Zahalka F, *et al*. Microstructure and performance of titanium oxide coatings sprayed by oxygen–acetylene flame. *Photochem Photobiol Sci* 2011, **10**: 403–407.

[9] Lima RS, Marple BR. Process–property–performance relationships for titanium dioxide coatings engineered from nanostructured and conventional powders. *Mater Design* 2008, **29**: 1845–1855.

[10] Fauchais P, Vardelle A, Dussoubs B. Quo vadis thermal spray? *J Therm Spray Techn* 2001, **10**: 44–66.

[11] Bozorgtabar M, Rahimipour M, Salehi M. Novel photocatalytic TiO_2 coatings produced by HVOF thermal spraying process. *Mater Lett* 2010, **64**: 1173–1175.

[12] Jeffery B, Peppler M, Lima RS, *et al*. Bactericidal effects of HVOF-sprayed nanostructured TiO_2 on pseudomonas aeruginosa. *J Therm Spray Techn* 2010, **19**: 344–349.

[13] George N, Mahon M, McDonald A. Bactericidal performance of flame-sprayed nanostructured titania–copper composite coatings. *J Therm Spray Techn* 2010, **19**: 1042–1053.

[14] Skopp A, Kelling N, Woydt M, *et al*. Thermally sprayed titanium suboxide coatings for piston ring/cylinder liners under mixed lubrication and dry-running conditions. *Wear* 2007, **262**: 1061–1070.

[15] Leivo J, Varis TE, Turunen E, *et al*. Influence of the elementary mixing scale on HVOF-sprayed coatings derived from nanostructured aluminosilicate/mullite feedstock. *Surf Coat Technol* 2008, **203**: 335–344.

[16] Ctibor P, Neufuss K, Chraska P. Microstructure and

abrasion resistance of plasma sprayed titania coatings. *J Therm Spray Techn* 2006, **15**: 689–694.

[17] ASTM International. ASTM G75-95. Standard Test Method for Determination of Slurry Abrasivity (Miller Number) and Slurry Abrasion Response of Materials (SAR Number). 1995.

[18] Reddy KM, Manorama SV, Reddy AR. Bandgap studies on anatase titanium dioxide nanoparticles. *Mater Chem Phys* 2003, **78**: 239–245.

[19] Moustakas NG, Kontos AG, Likodimos V, *et al*. Inorganic–organic core–shell titania nanoparticles for efficient visible light activated photocatalysis. *Appl Catal B*: *Environ* 2013, **130–131**: 14–24.

[20] Chen X, Liu L, Yu PY, *et al*. Increasing solar absorption for photocatalysis with black hydrogenated titanium dioxide nanocrystals. *Science* 2011, **331**: 746–750.

[21] Tsuyumoto I, Uchikawa H. Nonstoichiometric orthorhombic titanium oxide, $TiO_{2-\delta}$ and its thermochromic properties. *Mater Res Bull* 2004, **39**: 1737–1744.

[22] Barajas-Ledesma E, García-Benjume ML, Espitia-Cabrera I, *et al.* Determination of the band gap of TiO_2–Al_2O_3 films as a function of processing parameters. *Mat Sci Eng B* 2010, **174**: 71–73.

[23] Panpranot J, Kontapakdee K, Praserthdam P. Selective hydrogenation of acetylene in excess ethylene on micron-sized and nanocrystalline TiO_2 supported Pd catalysts. *Appl Catal A*: *Gen* 2006, **314**: 128–133.

[24] Tieng S, Kanaev A, Chhor K. New homogeneously doped Fe(III)–TiO_2 photocatalyst for gaseous pollutant degradation. *Appl Catal A*: *Gen* 2011, **399**: 191–197.